nature communications

Article

https://doi.org/10.1038/s41467-025-64435-6

Structural mechanism of the agonist binding on human TRPC3 channel

Received: 5 December 2024

Accepted: 15 September 2025

Published online: 22 October 2025

Check for updates

Yikun Chen[1,2,7], Jiahe Zang[1,7], Wenjun Guo[1,2,3,7], Jiaxuan Xu[1], Miao Wei[1], Li Quan[1], Min Zhu[4], Xiaole Zhao[5], Hailin Peng[5], Yakun Wan[4] & Lei Chen[1,2,3,6]

TRPC3/6/7 channels are cation channels that are directly activated by the second messenger diacylglycerol (DAG). These channels play crucial physiological roles and are implicated in various disease conditions; however, the binding mechanism of DAG to these channels remains incompletely understood. In this study, we present the structures of human TRPC3 in complex with DAG or synthetic activators, 4n and GSK1702934A. The structural analysis reveals that DAG binds at the L2 site, located near the pore on the extracellular side of TRPC3. Functional assays confirmed that the L2 site serves as the activating site for DAG. Notably, both 4n and GSK1702934A competitively bind to the same site, facilitating channel activation. Moreover, based on the pharmacophore identified from the DAG-bound structure, we found that monoacylglycerols (MAGs) are endogenous activators of TRPC3/6/7 channels, providing new insights into their regulatory mechanisms.

Canonical TRP channels (TRPC channels) are calcium-permeable, non-selective cation channels activated by receptor-mediated signaling[1]. In humans, there are six TRPC channel members: TRPC1, TRPC3, TRPC4, TRPC5, TRPC6, and TRPC7[1]. Based on their sequence homology and activation mechanism, TRPC3/6/7 can be grouped into one subfamily, which is directly activated by second messenger diacylglycerol (DAG)[2,3]. In contrast, the activation of TRPC4/5 by DAG is additionally regulated by PKC pathway and NHERF[4].

TRPC3/6/7 channels are widely distributed across various tissues and play significant roles in numerous physiological processes[1]. Notably, TRPC3 channels are highly expressed in the brain[5]. TRPC6 shows high expression levels in the placenta, heart, lungs, pancreas, kidneys, and brain[6], while TRPC7 is prominently found in the kidneys, pituitary gland, and brain[6]. Furthermore, TRPC3/6/7 channels are implicated in several diseases. In particular, TRPC6 channels are crucial for kidney podocyte physiology, and several gain-of-function mutations of the TRPC6 gene are associated with familial Focal Segmental Glomerulosclerosis (FSGS)[7,8].

Structural studies of homotetrameric TRPC3 and TRPC6 have revealed a two-layer architecture[9,10]. The transmembrane domain (TMD) consists of a central pore surrounded by voltage-sensor-like domains (VSLD), while the intracellular domain (ICD) is formed by linker helices, ankyrin repeat (AR) domains, and C-terminal helices[9,10]. Three calcium-binding sites (CBS) have been identified in TRPC3 and TRPC6[11]. CBS1, located in the ICD, plays an inhibitory role, whereas CBS3, found in the voltage sensor-like domain, serves as an activating site[11]. Various small molecular tool compounds are available for TRPC3, TRPC6, and TRPC7[1]. Previous structural studies have identified the binding sites for some of them. Inhibitors SAR7334 and AM-1473 bind at the inhibitor binding pocket A (IBP-A) within the VSLD of TRPC6, blocking the activating CBS3[11,12]. The activator AM-0883 binds at IBP-B at the subunit interface of the TRPC6 pore[12]. Additionally, the inhibitor BTDM binds at IBP-C between the VSLD and pore domain of TRPC6[10,11].

DAG is an endogenous activator for TRPC3, TRPC6, and TRPC7 channels[1]. It is produced by the phospholipase C (PLC) signaling

[1]State Key Laboratory of Membrane Biology, College of Future Technology, Institute of Molecular Medicine, Peking University, Beijing Key Laboratory of Cardiometabolic Molecular Medicine, Beijing, China. [2]Academy for Advanced Interdisciplinary Studies, Peking University, Beijing, China. [3]Peking-Tsinghua Center for Life Sciences, Peking University, Beijing, China. [4]Shanghai Novamab Biopharmaceuticals Co, Ltd, Shanghai, China. [5]Center for Nanochemistry, Beijing Science and Engineering Center for Nanocarbons, Beijing National Laboratory for Molecular Sciences, College of Chemistry and Molecular Engineering, Peking University, Beijing, China. [6]National Biomedical Imaging Center, Peking University, Beijing, China. [7]These authors contributed equally: Yikun Chen, Jiahe Zang, Wenjun Guo. e-mail: chenlei2016@pku.edu.cn

downstream of receptor activation, such as G protein-coupled receptors (GPCRs)[13]. Previous studies on TRPC3 have identified two lipid-binding sites, L1 and L2[9], in which L2 is at the same location as IBP-B. The development of light-sensitive OptoDArG has shown that G640 of TRPC3 is near the DAG binding site[14]. Further molecular dynamics simulations and mutagenesis studies suggest that DAG also binds at the L2 site[15]. Although insights into how DAG interacts with TRPC3, TRPC6, and TRPC7 are emerging, the detailed structural mechanism of DAG binding remains to be fully elucidated. Here, we present high-resolution structures showing the binding mode of DAG and other chemical activators at the L2 site of human TRPC3 (hTRPC3) channel. Moreover, these findings collectively lead to the identification of MAGs as hitherto unidentified endogenous activators of TRPC3/6/7.

Results

Structures of hTRPC3 in complex with three nanobodies

To facilitate biochemical and structural studies of hTRPC3, we generated nanobodies that recognize hTRPC3. We successfully identified three nanobodies, Nanobody 1-94 (Nb1-94), Nb1-25, and Nb3-37, which bind to hTRPC3 with high affinities (Supplementary Fig. 1). We reconstituted hTRPC3 into nanodiscs in the presence of calcium, along with each individual nanobody, for cryo-electron microscopy (cryo-EM) sample preparation. Subsequent single particle analysis yielded reconstructions at 2.25, 2.67, and 3.01 Å for hTRPC3 in complex with Nb1-94, Nb1-25, and Nb3-37, respectively (see Supplementary Figs. 2–4 and Supplementary Table 1).

All of the three nanobodies bind to the ICD of hTRPC3 but exhibit distinct stoichiometries (Fig. 1). Specifically, one hTRPC3 tetramer binds four Nb1-94 or Nb1-25 molecules (Fig. 1a, b, d, e) but two Nb3-37 molecules (Fig. 1g, h). Nb1-94 interacts with AR1 and AR2 domain of one subunit and C-terminal helix 2 (CH2) of the adjacent subunit (Fig. 1c). Nb1-25 engages with AR1 from one subunit and AR2-3 from an adjacent subunit (Fig. 1f). In contrast, Nb3-37 not only binds to the AR domains but also to CH2 (Fig. 1i). Notably, the binding of Nb3-37 results in the unwinding of the 806–811 region of the CH2 helix in two diagonally positioned subunits, while the CH2 of the adjacent subunits remain unchanged (Supplementary Fig. 4i). Consequently, only two structural epitopes on one hTRPC3 tetramer are available for Nb3-37 binding (Fig. 1g, h). Despite these localized conformational changes, the overall structure of hTRPC3 in the presence of the nanobodies remains similar to the previously determined structure of hTRPC3 in the presence of calcium[11] (PDB ID: 7DXB), where their ICD adopts a calcium-bound compact conformation and channel pore remains closed (Fig. 1a, d and g). Notably, the exceptional map quality of hTRPC3 in complex with Nb1-94 revealed the detailed binding mode of calcium at CBS1 (Fig. 1j–l). We found that calcium is chelated by four water molecules, the side chain of D798, the side chain of E73, and the main chain carbonyl group of E73, showing a heptacoordinated geometry (Fig. 1j–l).

DAG binds at the L2 site of hTRPC3

The cryo-EM map of hTRPC3 in complex with Nb1-94, at a resolution of 2.25 Å, reveals enhanced structural features compared to other available maps of hTRPC3. Notably, we observed a lipid-like density near the extracellular mouth of the hTRPC3 pore, referred to as the L2 site[9] (also known as the IBP-B site[16]) (Figs. 1a and 2). The shape and size of this density correspond closely to those of DAG (Supplementary Fig. 2i, j). To investigate the presence of DAG in the protein sample, we extracted lipids from the hTRPC3 protein purified through affinity chromatography and conducted mass spectrometry analysis (Supplementary Fig. 5). The results showed a markedly higher content of DAG in the hTRPC3 protein sample compared to the elution buffer control (Supplementary Fig. 5), with a notable presence of 1,2-dioleoyl-sn-glycerol (C18:1–C18:1 DAG) (Supplementary Fig. 5c and Supplementary Table 2). Moreover, we also confirmed the significant presence of DAG in the protein sample using an enzymatic DAG assay kit (Fig. 2a). These data collectively suggest that the density in the L2 site represents DAG. We modeled C18:1–C18:1 DAG into the observed density map (Fig. 2b–d). Due to the flexibility of the fatty acid tails of DAG, some atoms could not be confidently modeled (Fig. 2c, d). The model indicates that the free hydroxyl group at the C3 position of the glycerol moiety in DAG forms hydrogen bonds with E603 and K607 on the pore helix of one subunit of hTRPC3, as well as with N633 on the pore helix of an adjacent subunit (Fig. 2c, d). The C3-OH group is a distinguishing feature of DAG compared to other common glycerophospholipids, in which this position is typically linked to a phosphate group. Therefore, E603, K607, and N633 of hTRPC3 likely play critical roles in DAG recognition (Fig. 2c, d). Additionally, the glycerol moiety engages in hydrophobic interactions with W611 on the pore helix of one subunit, and Y636 and V637 of the S6 helix in the adjacent subunit (Fig. 2c, d). The fatty acid at the C1 position interacts with F606 on the pore helix of one subunit, while the fatty acid at the C2 position interacts with F610 on the pore helix of one subunit and Y636, G640, I641, V644, and T645 on the S6 helix of the adjacent subunit (Fig. 2c, d). The residues that interact with the glycerol moiety are absolutely conserved among hTRPC3, hTRPC6, and hTRPC7 (Fig. 2e). This is consistent with the findings, where DAG densities of similar shape and location were observed in hTRPC3 in complex with the other two nanobodies (Fig. 1d, g), as well as in hTRPC3 and hTRPC6 in earlier studies[9,11,12] (Supplementary Fig. 6). In contrast, several DAG-binding residues are not conserved between TRPC3/6/7 and TRPC4/5 (Fig. 2e), which correlates with the different binding poses of DAG between hTRPC3 and hTRPC5[16] (Supplementary Fig. 7). Moreover, in the map of hTRPC6 in complex with the agonist AM-0883, the DAG density is replaced by the density of the AM-0883 molecule[12] (Supplementary Fig. 6d, e), suggesting their competitive binding behavior.

Both GSK1702934A and 4n bind at L2 site of hTRPC3

To investigate the binding modes of other synthetic hTRPC3 activators, we performed cryo-electron microscopy (cryo-EM) studies of hTRPC3 in complex with two potent agonists, GSK1702934A[17] and 4n[18], under low-calcium conditions. The electron density maps for hTRPC3 in the GSK1702934A-bound and 4n-bound states reached resolutions of 2.7 Å and 3.3 Å, respectively (Figs. 3 and 4, Supplementary Figs. 8 and 9, and Supplementary Table 1).

The overall architecture of hTRPC3 with these activators bound is similar to that of the low-calcium state structure (PDB ID: 7DXC), with the intracellular domain (ICD) exhibiting a loosely packed conformation and the channel pore in closed state[11]. The root-mean-square deviation (RMSD) between the GSK1702934A-bound state and the low-calcium state hTRPC3 is 0.794 Å, while the RMSD between the 4n-bound state and the low-calcium state hTRPC3 is 0.621 Å. Both maps revealed prominent densities for the agonists at the L2 site (Figs. 3c and 4c), positioned similarly to AM-0883 on TRPC6[12].

The GSK1702934A molecule bound at the L2 site is surrounded by the pore helix from one subunit and the S6 from the adjacent subunit (Fig. 3c–e). The E603 on the pore helix and N633 on the S6 helix form polar contacts with the benzimidazolyl group of GSK1702934A (Fig. 3d–f). The W611 on the pore helix forms a hydrogen bond with the carbonyl of GSK1702934A. V637, I641 on the S6 helix and Y636, F606, K607, F610, W611 on the pore helix show hydrophobic interactions with GSK1702934A (Fig. 3d–f). Our observation is in agreement with previous findings showing that the mutations of E603D, K607R, N633Q, and Y636W significantly reduce the apparent affinity of GSK1702934A[19]. Notably, although GSK1702934A binds to a site that is similar to the one identified by docking studies, the binding pose is distinct from the computational model[19]. Particularly, in contrast to docking studies[19], the benzimidazolyl group of GSK1702934A does not form interactions with K629 and E632 but is close to E603 and F606 (Fig. 3d–f). Residues that interact with GSK1702934A are highly

https://doi.org/10.1038/s41467-025-64435-6

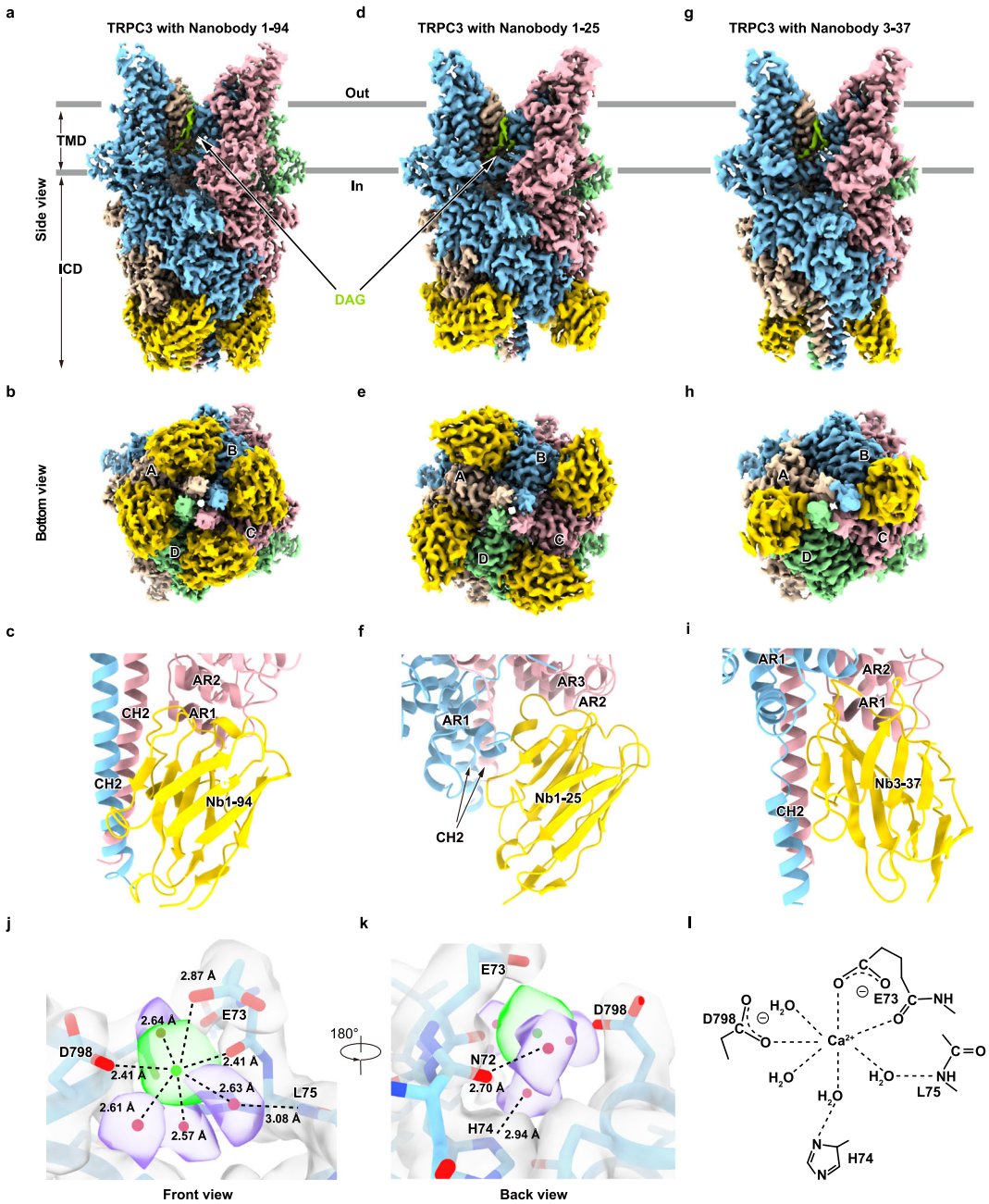

Fig. 1 | Cryo-EM structures of the hTRPC3-Nb complex. a, **b** Cryo-EM density map of the hTRPC3-Nb1-94 complex shown in side view (**a**) and bottom view (**b**). Subunits A, B, C, and D are colored in yellow, blue, pink, and green, respectively. Nanobodies are colored in gold. DAG is colored in bright green. TMD transmembrane domain, ICD intracellular cytosolic domain. There are four Nb1-94 bound on one hTRPC3 tetramer. **c** Close-up view of the binding site of Nb1-94 on hTRPC3. hTRPC3 and Nb1-94 are shown in cartoons. Nb1-94 binds to the CH2 in the B subunit and AR1 and AR2 in the C subunit of the hTRPC3 tetramer. **d**, **e** Cryo-EM density map of the hTRPC3-Nb1-25 complex shown in side view (**d**) and bottom view (**e**). There are four Nb1-25 bound on one hTRPC3 tetramer. **f** Close-up view of the binding site of Nb1-25 on hTRPC3. hTRPC3 and Nb1-25 are shown in cartoons. Nb1-25 binds to the AR1 in the B subunit and AR2 and AR3 in the C subunit of the hTRPC3 tetramer. **g**, **h** Cryo-EM density map of the hTRPC3-Nb3-37 complex shown in side view (**g**) and bottom view (**h**). There are two Nb3-37 bound on one hTRPC3 tetramer. **i** Close-up view of the binding site of hTRPC3 and Nb3-37. hTRPC3 and Nb3-37 are shown in cartoons. Nb3-37 binds to the CH2 and AR domains of the B and C subunits, altering the conformation of some helices and transforming the hTRPC3 tetramer from C4 symmetry to C2 symmetry. **j**, **k** The electron density of the calcium at CBS1 and nearby residues in the front view (**j**) and back view (**k**) in the map of hTRPC3 in complex with Nb1-94. The densities of TRPC3 are colored in gray, the calcium ion in green, and water in purple. The nearby residuals are shown as sticks, and the distance between atoms are marked out. **l** Schematic diagram of the interaction in the CBS1 region.

conserved among TRPC3/6/7 but not in TRPC4/5 (Fig. 3g), in agreement with the high selectivity of GSK1702934A for TRPC3/6/7 over TRPC4/5. The only different amino acid, I641 of hTRPC3 (corresponding to V710 of hTRPC6), may be responsible for the small difference in the potency of GSK1702934A between hTRPC3 and hTRPC6[17]. It is reported that the G640A mutation of hTRPC3 can increase the potency of GSK1702934A and its structural (benzimidazole) analog BI-2[20], probably because the G640A can increase the hydrophobic interactions between TRPC3 and GSK1702934A.

Although 4n has a distinct chemical structure compared to GSK1702934A and AM-0883, 4n also binds to the L2 site (Fig. 4a, b). 4n interacts with F577 and M580 on the S5 helix, E603, F606, F610, and W611 on the pore helix from one subunit, and N633, Y636, and V637 on

https://doi.org/10.1038/s41467-025-64435-6

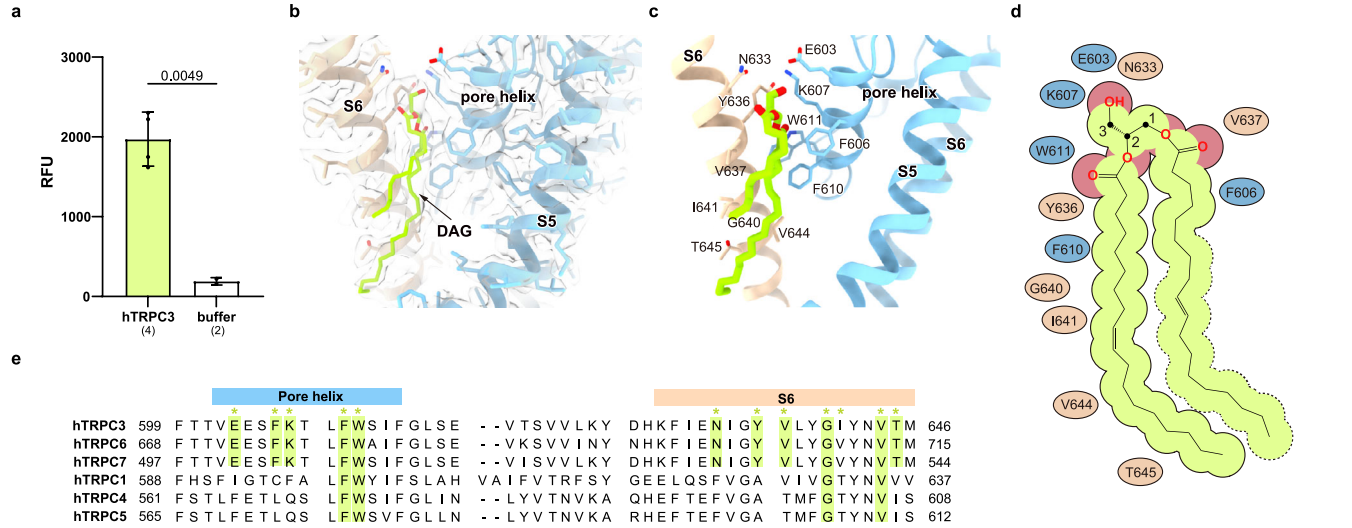

Fig. 2 | The binding site of DAG on hTRPC3. a The content of 1,2-dioleoyl-sn-glycerol in hTRPC3 protein sample and buffer control. hTRPC3 protein was purified using amylose resin and subsequently buffer-exchanged by ultrafiltration. The data are shown as the mean ± SD. The number of the analyzed TRPC3 protein sample is 4 and the number of buffer control sample is 2, biological replicates. The data were analyzed using one-tailed *t*-test and the *p*-value is 0.0049. Source data are provided as a Source Data file. **b** The electron density of the DAG and nearby residues shown in the semi-transparent surface. **c** The close-up view of the DAG-binding pocket of hTRPC3. DAG is shown as sticks, and hTRPC3 is shown as cartoon. **d** Cartoon representation of the interactions between hTRPC3 and DAG. The dashed lines represent the regions that were not modeled due to their flexibility. **e** Sequence alignment among TRPC1/4/5 and TRPC3/6/7 is shown. The residues that interact with DAG are marked by light green asterisks. Conserved residues are colored in light green. The corresponding domains are labeled above the sequence.

the S6 helix from the adjacent subunit (Fig. 4c–e). Among them, E603 on the pore helix, and N633 on the S6 helix form polar contacts with the central pyrimidine group of 4n. Side chains of Y636, V637 on the S6 helix, and F606, K607, and F610 on the pore helix form hydrophobic interactions with the piperidine tail of 4n (Fig. 4c–e). The W611 on the pore helix also forms a hydrogen bond with 4n. Residues F577 and M580 on the S5 helix are close to the trifluoromethyl phenyl head of 4n and may also contribute to the binding of 4n (Fig. 4f). These observations are in agreement with the functional data showing that mutations of E603, N633, Y636, and K607 (corresponding to E672, N702, Y705, and K676 of hTRPC6, respectively) all reduce the potency of a 4n-mimic M085[19]. Particularly, the N633Q (corresponding to hTRPC6 N702Q), Y636W (corresponding to hTRPC6 Y705W), and E603C (corresponding to hTRPC6 E672C) dramatically decrease the potency of M085[19], emphasizing the importance of these residues on the activation effect of 4n. Among all the residues close to 4n, the F577 of hTRPC3 (corresponding to V646 of hTRPC6) may contribute to the slightly higher selectivity of 4n for TRPC3 over TRPC6 because all the other residues are identical (Fig. 4g).

Comparison of the TMD structure of hTRPC3 bound to Nb1-94 with that bound to GSK1702934A or 4n reveals a high degree of structural similarity, with RMSD values of 0.760 Å and 0.463 Å, respectively. Structural alignments using TMD showed that the binding site of DAG, especially the glycerol moiety, overlaps with GSK1702934A and 4n, suggesting they compete for binding to the same L2 site (Supplementary Fig. 6).

DAG binding at L2 activates hTRPC3

While we observed DAG at the L2 site of hTRPC3 in our cryo-EM structures, it remains unclear whether DAG binding at this site activates the hTRPC3 channel or simply plays a structural role. To explore this, we mutated the DAG-binding residues on hTRPC3 to assess the responses of these mutants to DAG. Specifically, we generated E603A, K607A, and V637A mutants, targeting residues that interact with the glycerol moiety of DAG (Fig. 5a). On one hand, we utilized carbachol (CCh) to activate endogenously Gq-coupled muscarinic acetylcholine receptors, which subsequently activate phospholipase C (PLC) to produce DAG at the inner leaflet of plasma membrane to activate hTRPC3. On the other hand, we applied the exogenous DAG analogue 1-oleoyl-2-acetylglycerol (OAG) on the extracellular side of the cell for hTRPC3 activation. Our results indicated that the activation of these mutant hTRPC3 channels by CCh and OAG was largely abolished compared to wild-type hTRPC3 (Supplementary Fig. 10). To confirm that these mutant channels were properly trafficked to the plasma membrane and retained normal gating capabilities, we used GSK1702934A or 4n to activate them. We found that activation by GSK1702934A or 4n was largely preserved (Fig. 5b–e and Supplementary Fig. 10), contrasting sharply with the impaired activation observed with CCh and OAG. Collectively, these data suggest that the L2 site, located in the outer leaflet of the membrane, serves as the binding site for DAG, which activates the hTRPC3 channel. This finding aligns with previous studies showing that mutations such as G640A and Y636F in hTRPC3 decreased PLC-mediated activation and altered the kinetics of photoactivation by the photo-switchable DAG analogue OptoDArG[14,15,20]. Similarly, in hTRPC6, mutations E672A, F675A, W680A, N702A, Y705A, and V706A completely abolished the response of hTRPC6 to OAG while maintaining normal membrane surface expression[12].

Monoacylglycerols are agonists for TRPC3/6/7 channels

The observed binding mode of DAG to hTRPC3 (Fig. 2), along with our mutagenesis results (Fig. 5 and Supplementary Fig. 10), indicates that the free hydroxyl group at the C3 position of the glycerol moiety is a key determinant for hTRPC3 binding and activation. Furthermore, the DAG analog OAG, which features a short acetyl group in place of a long fatty acid tail, serves as a strong agonist for TRPC3/6/7 channels (Fig. 5f), indicating that two fatty acid tails may not be both necessary for the activation of TRPC channels. This leads us to hypothesize that closely related lipids, such as 1-monoacylglycerol (1-MAG) and 2-monoacylglycerol (2-MAG), which also feature a free C3-OH group but only one fatty acid tail (Fig. 5e), may also serve as activators of hTRPC3. Our whole-cell patch-clamp experiments demonstrated that both 1-oleoyl-glycerol (1-MOG) and 2-oleoyl-glycerol (2-MOG) robustly evoked TRPC3 channel currents with a slow off-rate (Fig. 5g).

https://doi.org/10.1038/s41467-025-64435-6

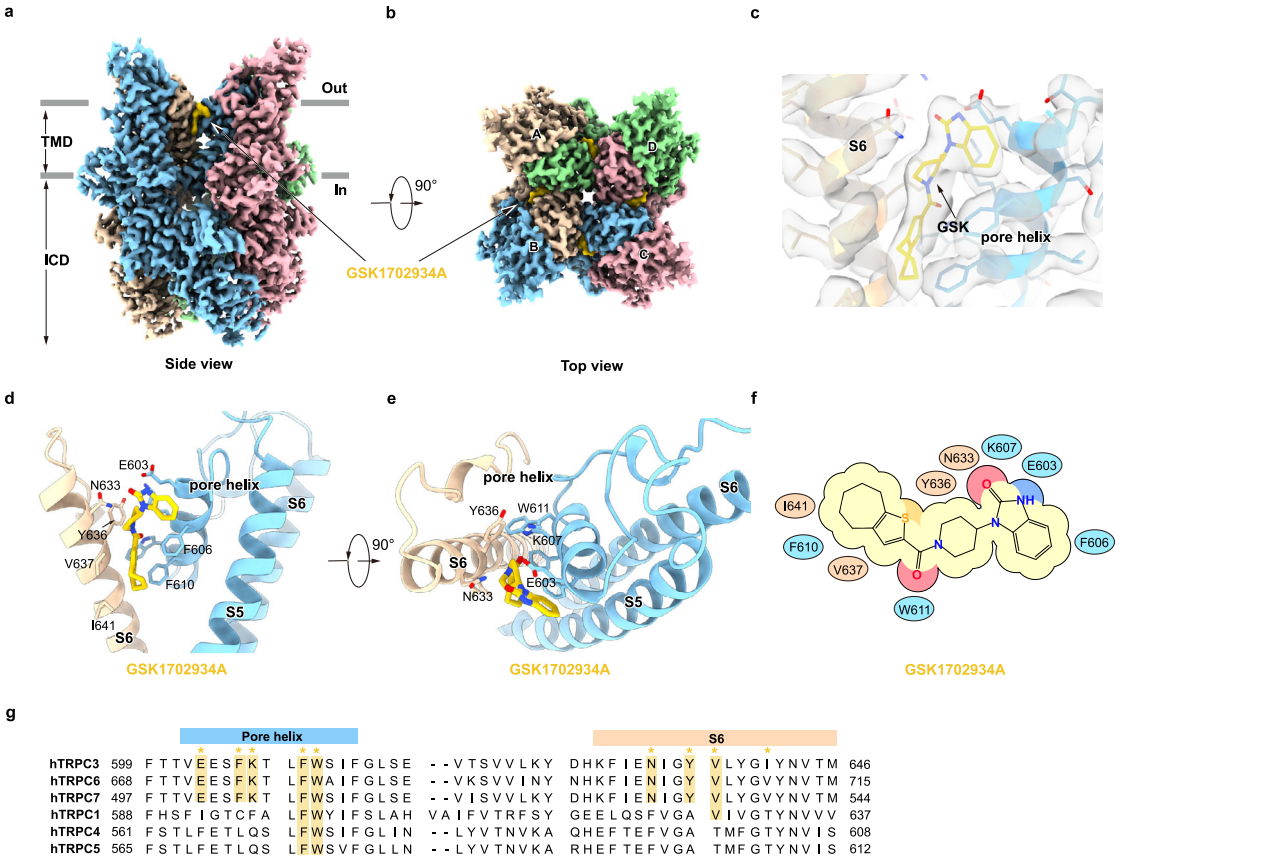

Fig. 3 | GSK1702934A binding sites in hTRPC3. a, **b** Cryo-EM density maps of GSK1702934A-bound state hTRPC3 shown in side view (**a**) and top view (**b**). Subunits A, B, C, and D are colored in yellow, blue, pink, and green, respectively. Ligand GSK1702934A is colored in gold. The approximate boundary of the cell membrane is indicated by gray lines. TMD transmembrane domain, ICD intracellular cytosolic domain. **c** Densities of GSK1702934A and nearby residues shown in side view. Densities are shown as grey surfaces. GSK1702934A is shown as sticks, and hTRPC3 is shown as cartoon. Both are colored the same as in (**a**). **d**, **e** Close-up view of the GSK1702934A-binding site. The GSK1702934A molecule and the side chains of its interacting residues are shown as sticks. **f** Cartoon representation of the interactions between GSK1702934A and hTRPC3. S6 of subunit A and S5, S6, pore helices of subunit B are represented as yellow ovals and blue ovals, respectively. Residues that interact with GSK1702934A are labeled inside the ovals. **g** Sequence alignment among TRPC1/4/5 and TRPC3/6/7 is shown. The residues that interact with GSK1702934A are marked by gold asterisks. Conserved residues are colored in gold. The corresponding domains are labeled above the sequence.

This aligns with the presence of the lipophilic fatty acid tails in MAG, which may insert into the plasma membrane and slow the dissociation process (Fig. 5f). The slow off-rate of these MAGs hindered us from accurately measuring their EC_{50} values. However, we found that 25 μM of either 1-MOG or 2-MOG could activate hTRPC3 to levels comparable to those achieved with 5 μM OAG (Fig. 5g). Moreover, we found that 1-MOG and 2-MOG can also activate TRPC6 and TRPC7 channels (Fig. 5h, i), but not TRPC5 channel (Supplementary Fig. 10i). Collectively, these findings suggest that MAGs function as agonists of TRPC3, TRPC6, and TRPC7.

Discussion

The key precursor of DAG, $PI(4,5)P_2$, is predominantly localized in the inner leaflet of the plasma membrane[21]. Upon receptor activation, phospholipase C (PLC) on the intracellular side of the membrane hydrolyzes $PI(4,5)P_2$, resulting in the generation of DAG[13] (Supplementary Fig. 11). Consequently, newly produced DAG is initially situated in the inner leaflet of the plasma membrane (Supplementary Fig. 11). The inner leaflet localization of the initially produced DAG appears to conflict with our cryo-EM structural data and mutagenesis results, which indicates that the activating DAG-binding site is near the extracellular mouth of the TRPC3 pore and within the outer leaflet of plasma membrane. However, it has been demonstrated that DAG can freely flip-flop between the inner and outer leaflets of the plasma membrane[22]. This translocation occurs with rapid kinetics, compatible with the activation kinetics of TRPC channels by GPCRs[23]. These findings suggest that receptor activation generates DAG in the inner leaflet, which subsequently translocates to the outer leaflet to activate TRPC3/6/7 channels (Supplementary Fig. 11). This mechanism is further supported by evidence showing that DAG analogs, such as OAG, can activate TRPC3/6/7 from either side of the plasma membrane[2].

DAG is a signaling molecule that typically exists at low concentrations in resting cells, resulting in TRPC3/6/7 channels being only partially occupied by DAG to maintain their closed state. However, the structures of hTRPC3 in complex with nanobodies presented here (Fig. 1), along with several previous structures of hTRPC3 and hTRPC6[9–11], consistently show DAG bound at the L2 site. We speculate that the high occupancy of DAG on purified TRPC channels may be due to the cell culture, cell harvesting, or protein purification process, which likely activates PLC and significantly increases the DAG concentration in the system.

High-resolution cryo-EM structures have elucidated the binding mode of DAG, revealing that its C3-OH-free glycerol group is a critical chemical determinant for the binding and activation of TRPC3/6/7. This insight has led to the identification of MAGs as direct activators of these channels (Fig. 5). MAGs, primarily produced during lipolysis, are widely distributed throughout the body and play essential roles in various physiological processes[24]. For instance, MAGs are crucial in pancreatic β cells, where they regulate glucose-stimulated insulin release. Exogenous MAGs have been shown to stimulate insulin secretion, with

https://doi.org/10.1038/s41467-025-64435-6

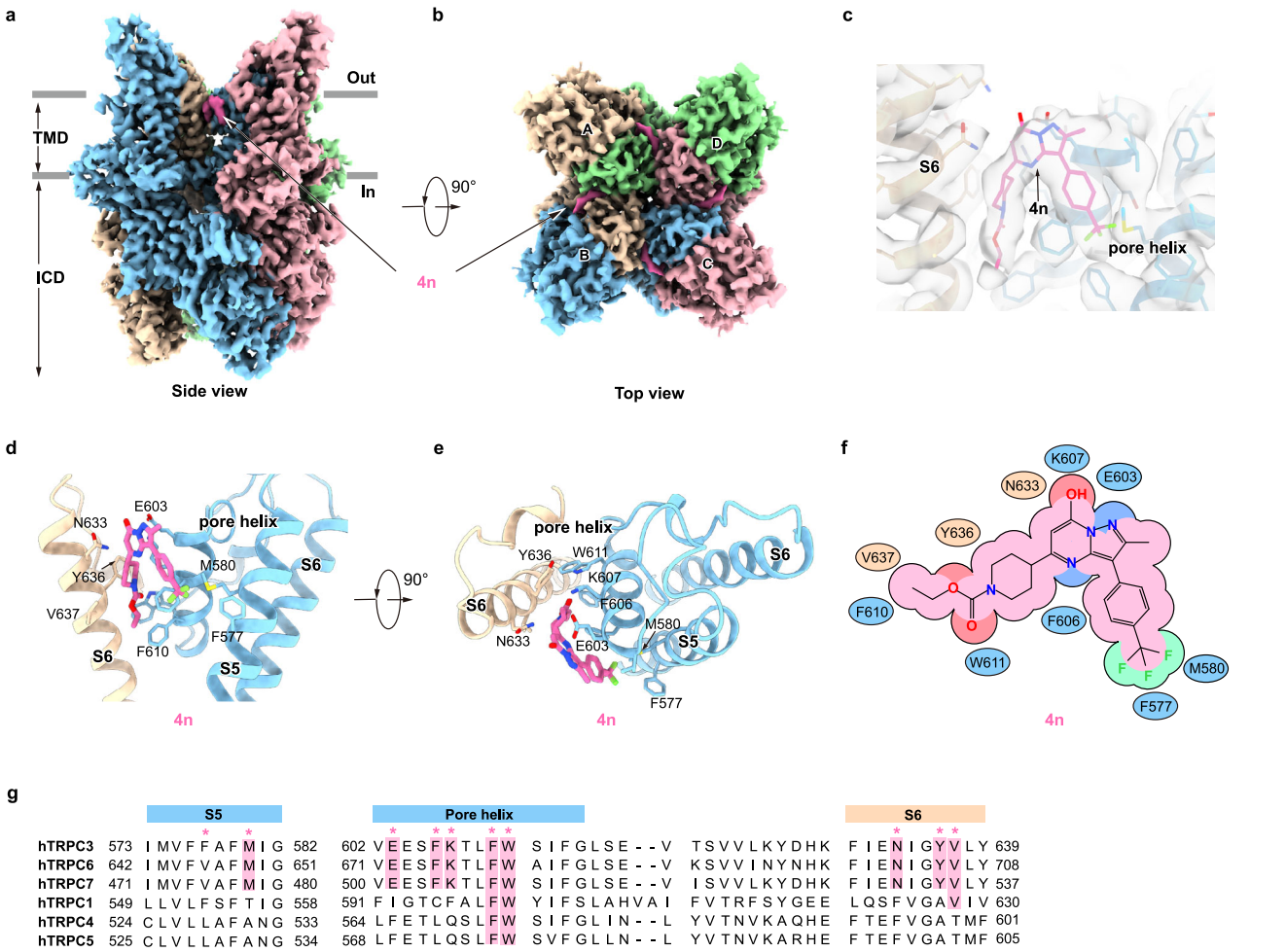

Fig. 4 | 4n binding sites in hTRPC3. a, **b** Cryo-EM density maps of 4n-bound state hTRPC3 shown in side view (**a**) and top view (**b**). Subunits A, B, C, and D are colored in yellow, blue, pink, and green, respectively. Ligand 4n is colored in magenta. The approximate boundary of the cell membrane is indicated by gray lines. TMD transmembrane domain, ICD intracellular cytosolic domain. **c** Densities of 4n and nearby residues shown in side view. Densities are shown as grey surfaces. Ligand 4n is shown as sticks, and hTRPC3 is shown as cartoon. Both are colored the same as in (**a**). **d**, **e** Close-up view of the 4n-binding site. The 4n molecule and the side chains of its interacting residues are shown as sticks. **f** Cartoon representation of the interactions between 4n and hTRPC3. S6 of subunit A and S5, S6, pore helices of subunit B are represented as yellow ovals and blue ovals, respectively. Residues that interact with 4n are labeled inside the ovals. **g** Sequence alignment among TRPC1/4/5 and TRPC3/6/7 is shown. The residues that interact with 4n are marked by magenta asterisks. Conserved residues are colored in magenta. The corresponding domains are labeled above the sequence.

Munc13-1 acting as one of the sensors for MAGs[25]. Although several receptors for MAGs have been determined[24–26], the identification of MAGs as endogenous agonists of TRPC3/6/7 channels establishes a mechanistic link between the physiological functions of MAGs and the activity of these channels. Particularly, TRPC3 is also expressed in pancreatic β cells, and the inhibition or knockout of TRPC3 in mice results in impaired insulin secretion and glucose intolerance[27]. This suggests that TRPC3 may play a positive role in MAG-facilitated insulin secretion in pancreatic β cells. The physiological significance of MAG as the agonists of TRPC3/6/7 awaits further studies.

Methods

Constructs

The cDNA of hTRPC3 was cloned into a modified N-terminal GFP-tagged BacMam vector for electrophysiology assay as described previously[10]. The cDNA of WT full-length hTRPC3 was inserted into an N-terminal GFP-MBP (Maltose Binding Protein)-tagged BacMam vector for protein purification. The CDS of nanobodies were cloned into the pET21 vector with an N-terminal pelB signal sequence followed by an MBP tag and an HRV 3C site, and with the C-terminal was tagged by Myc-ALFA-His tags.

Cell culture

Sf9 insect cells (Thermo Fisher Scientific) were cultured in SIM SF (Sino Biological) at 27 °C. FreeStyle 293F suspension cells (Thermo Fisher Scientific) were cultured in FreeStyle 293 medium (Thermo Fisher Scientific) supplemented with 1% fetal bovine serum (FBS, VisTech), 67 μg/mL penicillin (Macklin), and 139 μg/mL streptomycin (Macklin) at 37 °C with 6% CO_2 and 70% humidity. The cell lines were routinely checked to be negative for mycoplasma contamination, but have not been authenticated.

Electrophysiology

For whole-cell recordings of TRPC3/6/7, the pipette solution was 120 CsMe (Cesium methanesulfonate), 25 CsCl, 2 $MgCl_2$, 1 $CaCl_2$, 2 EGTA, and 30 HEPES (pH = 7.4 adjusted by CsOH) in mM, in which the free calcium was measured as 106 nM. The bath solution contains 140 NaCl, 5 CsCl, 2 $MgCl_2$, 1 EDTA, 2 EGTA, 10 Glucose, and 10 HEPES (pH = 7.4, adjusted by NaOH) in mM.

For whole-cell recordings of TRPC5, the pipette solution was 110 CsMe (Cesium methanesulfonate), 25 CsCl, 2 $MgCl_2$, 1 EDTA, 2 EGTA, and 30 HEPES (pH = 7.4 adjusted by CsOH) in mM. The bath solution contains 140 NaCl, 5 CsCl, 2 $MgCl_2$, 1 EDTA, 2

https://doi.org/10.1038/s41467-025-64435-6

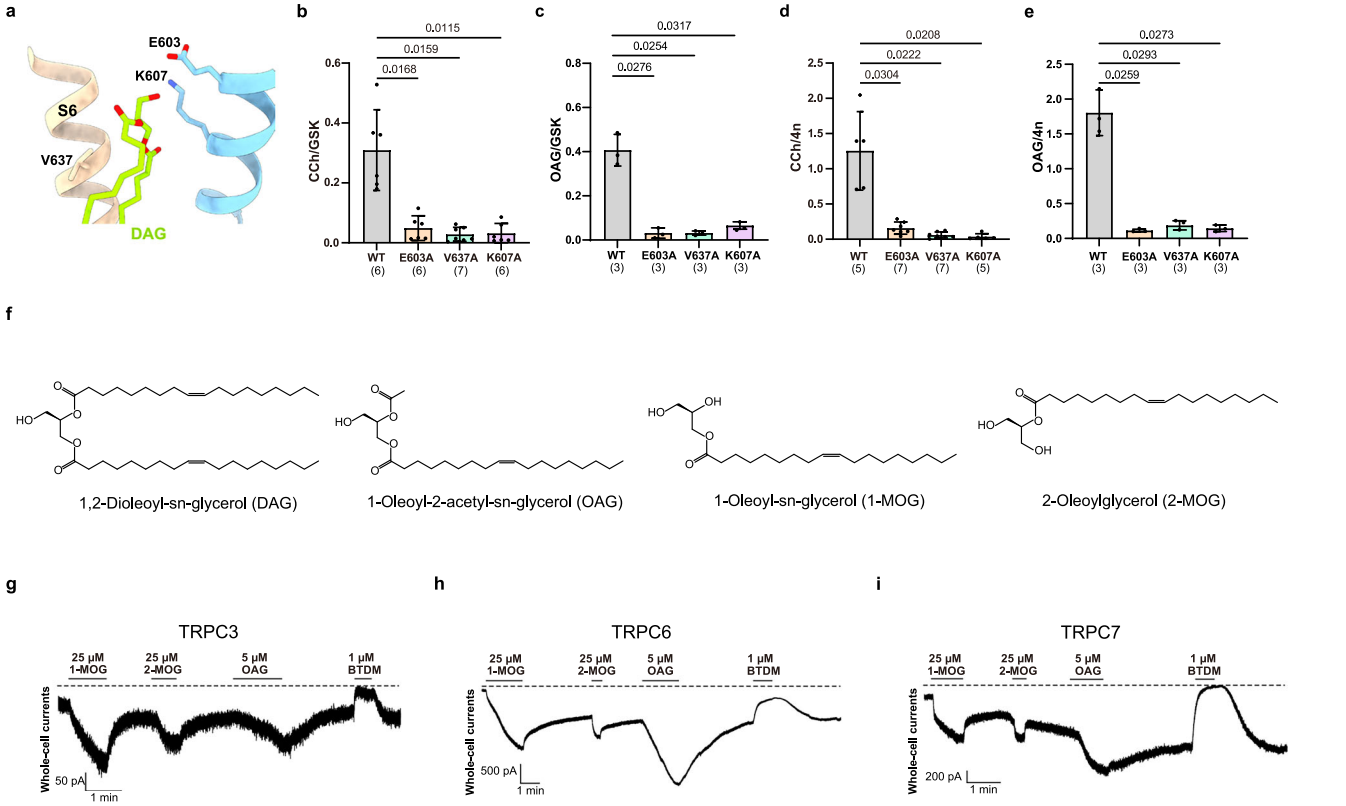

Fig. 5 | DAG and MAG bind to the L2 site for channel activation. a Close-up view of DAG at the L2 site. The mutated amino acids on hTRPC3 are shown as sticks. DAG is colored in green. TRPC3 is colored in blue. **b** The ratio of peak currents activated by CCh and GSK1702934A in wild-type, E603A, K607A, and V637A under whole-cell mode at −60 mV. The calculation method for the activation current is described in detail in Supplementary Fig. 10. The number of biological replicates in each group is indicated below the genotype. The data are shown as the mean ± SD. The data were analyzed using Brown–Forsythe and Welch ANOVA tests, and the multiple comparisons between each group were analyzed using Dunnett's T3 multiple comparisons tests with *p*-values indicated above the corresponding groups. Source data are provided as a Source Data file. **c** The ratio of peak currents activated by OAG and GSK1702934A in wild-type, E603A, K607A, and V637A under whole-cell mode at −60 mV. The calculation, annotation, and statistical analyses were identical to those described in (**b**). Source data are provided as a Source Data file. **d** The ratio of peak currents activated by CCh and 4n in wild-type, E603A, K607A, and V637A under whole-cell mode at −60 mV. The calculation, annotation, and statistical analyses were identical to those described in (**b**). Source data are provided as a Source Data file. **e** The ratio of peak currents activated by OAG and 4n in wild-type, E603A, K607A, and V637A under whole-cell mode at −60 mV. The calculation, annotation, and statistical analyses were identical to those described in (**b**). Source data are provided as a Source Data file. **f** Chemical structures of DAG, OAG, 1-MOG, and 2-MOG. **g**–**i**. Macroscopic currents of wild-type hTRPC3/6/7 recorded in the whole-cell mode. Zero current is indicated by a dashed line. The duration of ligand application is indicated by a solid line above. Source data are provided as a Source Data file.

EGTA, 10 Glucose, and 10 HEPES (pH = 7.4, adjusted by NaOH) in mM.

The concentration of Carbachol (CCh, HarveyBio, C33526), 4n (Dizal Pharmaceutical), GSK1702934A (Shanghai Universal Biotech, 6508), 1-Oleoyl-2-acetyl-sn-glycerol (OAG, Sigma, O6754), 1-Oleoyl-rac-glycerol (1-MOG, Sigma, M7765), 2-Oleoylglycerol (2-MOG, TargetMol, T37526), BTDM (Dizal Pharmaceutical), and (-)-Englerin A (EA, Sigma, PHL82530) used in patch-clamp are marked out in the figures.

Patch electrodes were pulled by a horizontal microelectrode puller (P-1000, Sutter Instrument Co., USA) to a tip resistance of 2.0–4.0 MΩ. An MPS-2 perfusion system (Yibo Company, Wuhan, China) was used for buffer change. The TRPC currents were recorded at a holding potential of −60 mV through an Axopatch 200B amplifier (Axon Instruments, USA). The currents with amplitudes greater than 150 pA were used for further analysis. Data were further low-pass filtered by pCLAMP 10.4 software. Plot the current traces using Origin 2024. Peak currents were statistically analyzed in GraphPad Prism 9, and then labeled the scale bars.

Nanobody selection

Recombinant nanobodies against hTRPC3 were provided by Shanghai Novamab Biopharmaceuticals Co. Ltd. These nanobodies were further screened against hTRPC3 using pull-down assay and FSEC with GFP-tagged hTRPC3. Nb1-94, Nb1-25, and Nb3-37 were selected because they can bind hTRPC3 protein in both assays.

Expression and purification of nanobody

Each nanobody construction was transformed to *E. coli* NiCo21 (DE3). Cells were cultured in LB medium at 37 °C. When the cell density reached OD600 = 0.6, the culture was cooled to 28 °C for 40 min. After that, 1 mM isopropyl-β-d-thiogalactoside (IPTG) was added and incubated for 16 h at 28 °C.

The nanobody was extracted by osmotic shock from the periplasmic space. The cell pellet cultured in 1 L of LB medium was resuspended with 24 mL of hyperosmotic buffer [0.5 M sucrose, 0.2 M Tris (pH 8.0 at 4 °C), 0.5 mM EDTA] and incubated at 4 °C for 30 min. Then, 48 mL of hypoosmotic buffer (1 mM $MgCl_2$ in ddH_2O) was added and incubated at 4 °C for 1 h. After centrifuging at 20,000 × *g* (JA-20, Beckman), 4 °C for 20 min, the supernatant was collected and supplemented with 150 mM NaCl, 1.4 mM $MgCl_2$, and 20 mM imidazole, then loaded twice on the 1 mL Ni-NTA column. The column was washed with 20 mM Tris (pH 8.0 at 4 °C) and 500 mM NaCl, followed by 20 mM Tris (pH 8.0 at 4 °C), 150 mM NaCl, and 20 mM imidazole. The target protein was eluted with elution buffer containing 20 mM Tris (pH 8.0

at 4 °C) and 200 mM Imidazole (pH 8.0). The eluate was loaded onto a HiTrap Q HP column (Cytiva) and eluted with high-salt buffer [20 mM Tris (pH 8.0), 1 M NaCl] in a linear gradient using the AKTA pure system.

Estimation of nanobody binding affinity to hTRPC3

To estimate the binding affinity between hTRPC3 and nanobodies, we performed ELISA using purified nanobodies and biotinylated Avi-tagged hTRPC3. hTRPC3 protein was biotinylated in vitro by biotin-protein ligase BirA, which was expressed and purified in our lab. Briefly, 25 nM biotinylated hTRPC3 in TBSM buffer [20 mM Tris (pH 8.0 at 4 °C), 150 mM NaCl, 0.01% LMNG, 0.001% CHS] was added (50 μL/well) to streptavidin-coated 12-well strips (Beaver) and the samples were incubated on ice for 1 h. Unbound antigen was removed by washing with TBSM. Strips were then blocked with TBSM containing 2% FBS (TBSM-FBS) for 30 min. Myc-tagged nanobodies at varying concentrations (50 μL/well in TBSM) were added and incubated on ice for 1 h. Following a TBSM wash, rabbit anti-Myc antibody (YN5506; Immunoway; diluted 1:2500 in TBSM-FBS; 50 μL/well) was added and the samples were incubated on ice for 1 h to bind the Myc-tagged nanobodies. After another TBSM wash, goat anti-rabbit HRP-conjugated antibody (31460; Thermo Fisher Scientific; diluted 1:4000 in TBSM-FBS; 50 μL/well) was added and the samples were incubated on ice for 1 h. Strips were washed extensively with TBSM before adding 100 μL of ELISA developing buffer [51.5 mM Na_2HPO_4, 24.3 mM citric acid, 0.006% H_2O_2, 0.1 mg mL^{-1} TMB] and incubating at room temperature for 10 min. The reaction was stopped with 100 μL of 2 M H_2SO_4. Absorbance was measured at 450 nm and 630 nm using an Infinite M Plex plate reader (Tecan). The ELISA signal for each well was calculated by subtracting the 630 nm reading from the 450 nm reading. Nonspecific binding signals, determined from wells containing nanobodies but lacking antigen, were subtracted from the total binding signals to yield specific binding signals. All experiments were performed in triplicate. Binding affinities of the nanobodies were estimated by fitting the specific binding data to a four-parameter variable slope (Hill coefficient) dose-response curve using nonlinear regression in GraphPad Prism 9, with the bottom constraint set to be greater than zero.

Protein expression and purification

The protein expression and purification were followed by the protocol just as reported[11]. The BacMam virus of full-length hTRPC3 was prepared for protein expression[28]. HEK293F cells grown in FreeStyle 293 medium at 37 °C with a density of 3.0×10^6 /mL were infected by BacMam viruses. 10 mM sodium butyrate and 100 nM BTDM were added 8–12 h post-infection, and the temperature was lowered to 30 °C. Cells were collected 48 h post-infection and washed twice with TBS buffer before being frozen at −80 °C.

To prepare the sample of hTRPC3 in complex with 4n and GSK1702934A, cell pellets were solubilized in 10 mM MNG, 0.1% CHS, 100 nM BTDM, and protease inhibitors in TBS buffer and rotated at 4 °C for 1 h. After centrifugation at 40,000 rpm for 40 min in the Type 70 rotor (Beckman), the supernatant was loaded onto a column packed with amylose resin (NEB). The resin was washed with 40 μM GDN, 0.01 mg/mL soybean lipids, 100 nM BTDM, 10 mM $MgCl_2$, 1 mM ATP, and 4 mM DTT in TBS buffer to remove heat shock proteins. Protein was eluted with 100 mM maltose in TBS buffer supplemented with 40 μM GDN, 0.01 mg/mL soybean lipids, 100 nM BTDM, and 4 mM DTT. The concentrated protein was added 1 mM EDTA and 1 mM EGTA and incubated with H3CV protease and PNGase F at 4 °C overnight. Then the concentrated protein was loaded onto Superose-6 increase (GE Healthcare) running in TBS buffer supplemented with 40 μM GDN, 0.01 mg/mL soybean lipids, 100 nM BTDM, 1 mM EDTA, and 1 mM TCEP for further purification. The peak fractions containing tetrameric hTRPC3 channel protein were collected for nanodisc assembly. After assembly, the mixture was loaded onto a Superose-6 increase column running in TBS containing 1 mM EDTA and 1 mM TCEP to remove empty nanodiscs. The peak fractions that contain the tetrameric hTRPC3 channel in nanodiscs were combined and concentrated for cryo-EM studies.

To prepare the sample of hTRPC3 in complex with nanobodies, cell pellets were solubilized in 10 mM MNG, 0.1% CHS, and protease inhibitors in TBS buffer and rotated at 4 °C for 1 h. After centrifugation at 40,000 rpm for 40 min in the Type 50.2 Ti (Beckman Coulter). The supernatant was loaded onto a column packed with amylose resin (NEB). The resin was washed with 40 μM GDN, 0.01 mg/mL soybean lipids, 10 mM $MgCl_2$, 1 mM ATP, and 4 mM DTT in TBS buffer to remove heat shock proteins. Protein was eluted with 80 mM maltose in TBS buffer supplemented with 40 μM GDN, 0.01 mg/mL soybean lipids, and 4 mM DTT. The concentrated protein was added to the purified Nanobody in a molar amount 1.2 times that of TRPC3 and assembled the nanodisc together. The mixture was incubated with PreScission protease at 4 °C overnight. After assembly, the mixture was loaded onto a Superose-6 increase (GE Healthcare) running in TBS buffer containing 1 mM TCEP to remove empty nanodiscs. The peak fractions that contain the tetrameric hTRPC3 channel in nanodiscs with nanobodies were combined and concentrated for cryo-EM studies.

Cryo-EM sample preparation

100 μM GSK1702934A was added to the purified tetrameric hTRPC3 nanodiscs with A280 = 1.7. The supernatant was collected after centrifuging at 40,000 rpm for 30 min, and then the protein was added on Quantifoil (0.6/1) gold grids coated with graphene oxide[29] for cryo-EM sample preparation. 100 μM 4n was added to the purified hTRPC3 nanodisc with A280 = 1.7. After centrifuging at 40,000 rpm for 30 min, the mixture was added on the Quantifoil (0.6/1) gold grids for cryo-EM sample preparation.

For hTRPC3-Nb1-94 complex, the purified tetrameric hTRPC3 nanodisc with Nb1-94 was concentrated to A280 = 1.5, and 1 mM $CaCl_2$ was added. After centrifuging at 40,000 rpm for 30 min, the supernatant was collected and added 0.5 mM fluorinated octyl maltoside (FOM), and then the protein was added on Quantifoil (0.6/1) Au grids coated with graphene[30] for cryo-EM sample preparation.

For hTRPC3-Nb1-25 and Nb3-37 complex, the purified tetrameric hTRPC3 nanodisc with Nb1-25 or Nb3-37 was concentrated to A280 = 1.8, and 1 mM $CaCl_2$ was added. After centrifuging at 40,000 rpm for 30 min, the supernatant was collected and added 0.5 mM FOM, then the protein was added on GIG (1/1) Cu grids coated with graphene oxide[31] for cryo-EM sample preparation.

Cryo-EM data collection

Cryo-EM grids were screened on the Talos Arctica electron microscope (Thermo Fisher Scientific) operating at 200 kV using a K2 camera (Thermo Fisher Scientific). The images of the screened grids of GSK1702934A-bound state hTRPC3 were collected on 300 kV Titan Krios (Thermo Fisher) with a K2 Summit direct electron camera (Thermo Fisher Scientific) and an energy filter set to a slit width of 20 eV at a magnification of 48,000× with a pixel size of 1.045 Å and the defocus ranging from −1.5 to −2 μm. Super-resolution movies (32 frames per movie) were collected automatically using Serial EM with a dose rate of 8 e^-/pixel/s on the detector and a total dose of 48 $e^-/Å^2$.

The screened grids of hTRPC3 nanodisc with 4n ligand were then transferred to the same 300 kV Titan Krios electron microscope at a magnification of 37,800× with a pixel size of 1.324 Å, and the defocus ranging from −1.0 to −3.0 μm, with a total dose about 50 $e^-/Å^2$ and a dose rate of 8 e^-/pixel/s on detector.

The screened grids of hTRPC3 nanodisc with Nb1-94 were then transferred to the 300 kV Titan Krios (Thermo Fisher Scientific) with a K3 camera (Gatan) and an energy filter set to a slit width of 20 eV at a

magnification of 60,000× with a pixel size of 0.833 Å, and the defocus ranging from −1.5 to −1.8 µm, with a total dose about 50 $e^-/Å^2$ and a dose rate of 22.15 e^-/pixel/s on detector.

The images of the screened grids of hTRPC3 nanodisc with Nb1-25 or Nb3-37 were collected on 300 kV Titan Krios (Thermo Fisher Scientific) with a K3 camera (Gatan) and an energy filter set to a slit width of 20 eV at a magnification of 47,000× with a pixel size of 1.067 Å and the defocus ranging from −1.5 to −1.8 µm. Super-resolution movies (32 frames per movie) were collected automatically using Serial EM with a dose rate of 21.46 e^-/pixel/s on the detector and a total dose of 70 $e^-/Å^2$.

Cryo-EM data processing

Both GSK1702934A-bound and 4n-bound state hTRPC3 datasets were first gain-corrected, motion-corrected, anisotropic magnification corrected, and dose-weighted by MotionCor2-1.3.2[32]. The selected micrographs were done CTF estimation using GCTF-1.18[33]. The low-pass filtered projections of the published map of hTRPC3 were used as templates for particle picking using Gautomatch (kindly provided by Kai Zhang). 2D and 3D classification were carried out using Relion 3.0[34]. Then the particles of the best class were imported into cryoSPARC-4.5.3[35] for seed-facilitated 3D classification[36]. To improve the resolution, multi-reference 3D classification was performed in cryoSPARC-4.5.3. The particles of the best class were selected for further local CTF and local refinement with C4 symmetry. The resolution estimation was based on the gold standard FSC 0.143 cut-off.

The data processing procedures for the hTRPC3-Nb1-94 complex followed the same strategy as described above. The selected micrographs were then imported into cryoSPARC-4.5.3. A round of template picking, 2D and 3D classification, and 3D refinement was performed in cryoSPARC-4.5.3. The resulting particles from the best class were used as "Seeds" for seed-facilitated 3D classification of particles extracted by Topaz. The particles selected after multi-reference 3D classification were subsequently used for final non-uniform refinement with C4 symmetry. The final particles were reboxed to achieve the optimal resolution. The resolution estimation was based on the gold standard FSC 0.143 cut-off.

The data processing procedures in the early stage of the hTRPC3-Nb1-25 complex and hTRPC3-Nb3-37 complex datasets were similar to the GSK1702934A-bound and 4n-bound state hTRPC3 described above. After carrying out 2D classification in Relion 3.0, the particles of the best classes were imported into cryoSPARC-4.5.3 for 3D classification. After seed-facilitated 3D classification, the particles of the best class were selected for further local CTF and local refinement. The hTRPC3-Nb1-25 complex dataset was carried out local refinement with C4 symmetry, and the hTRPC3-Nb3-37 complex dataset was carried out local refinement with C2 symmetry. The resolution estimation was based on the gold standard FSC 0.143 cut-off.

Model building, refinement, and validation

The GSK1702934A-bound and 4n-bound hTRPC3 models were manually rebuilt using Coot-0.9.8.93[37] based on the published models 7DXC and further refined using PHENIX1.19.2[38].

The Nb1-94-bound, Nb1-25-bound, and Nb3-37-bound hTRPC3 models were manually rebuilt using Coot-0.9.8.93 based on the published models 7DXB and further refined using PHENIX1.19.2.

Mass spectrum analysis

The purified hTRPC3 protein from amylose resin (NEB) was buffer-exchanged into LC–MS buffer (20 mM Tris-HCl, pH 8.0, 150 mM NaCl, 100 mM maltose, 40 µM GDN) using ultrafiltration spin columns (Millipore). The protein concentration was then determined using a BCA assay kit (Beyotime). For LC–MS analysis, 100 µL of hTRPC3 (20 µM) was mixed with 400 µL isopropanol, vortexed, and extracted by ultrasonication for 1 min. After centrifugation at 14,000 rpm for 10 min at 4 °C, the supernatant was transferred into a vial for further LC–MS analysis.

UPLC (Waters ACQUITY I-Class system) coupled with tandem ESI-Triple quadrupole mass spectrometry (Waters Xevo TQ-S Micro) was used to analyze 2 µL lipid extractants. An ACQUITY UPLC BEH Amide column (1.7 µm, 2.1 mm × 100 mm, Waters) was used in a HILIC mode for the separation of the lipid classes. The mobile phase of solvent A (10 mM ammonium acetate in 95:5 acetonitrile/water) and solvent B (10 mM ammonium acetate in 50:50 acetonitrile/water) was at a flow rate of 0.6 mL/min. The gradient program was as follows: 0 min 0.1% B, 2 min 20% B, 2–5 min 80% B, 5.1–8 min 99% B. The eluted lipids were directly introduced into the mass spectrometer with a desolvation temperature of 500 °C and a capillary voltage of 2.8 kV under positive ESI mode, and the source temperature was set at 120 °C. The analytes were monitored under full-scan mode with mass ranging from m/z 100 to 1200, combined with a daughter scan from m/z 50 to 650 for fragmentor of 638.6 (m/z), with a collision energy of 20 V. Masslynx 4.0 was used to acquire and screen MS and MS/MS data.

For lipid analysis, the LipidQuan™ (Waters) method was employed to detect lipid species in both purified protein samples and blank buffers. Two biological replicates were performed. After background subtraction using the blank controls, approximately 1200 lipid compounds were identified in the protein samples. Among them, a prominent peak with an area of ~17,325.38 and a retention time of 0.48 min was detected, corresponding to an MRM transition of 638.60 → 339.30. This strongly supports that the lipid bound to the protein is C18:1–C18:1 DAG. Additional minor peaks were also observed in the samples, as listed in Supplementary Table 2, but their peak areas were markedly smaller compared to C18:1–C18:1 DAG.

DAG content measurement

The purified hTRPC3 protein from amylose resin (NEB) was buffer-exchanged into 20 mM Tris-HCl, pH 8.0, 150 mM NaCl, 100 mM maltose, and 40 µM GDN using ultrafiltration spin columns (Millipore). The protein concentration was then determined using a BCA assay kit (Beyotime). A total of 70 ng hTRPC3 was used for DAG quantification following the protocol described in the DAG Assay Kit (Abcam).

Quantification and statistical analysis

Data processing and statistical analysis were conducted using the software GraphPad Prism 9. Statistical details could be found in the methods details and figure legends. The currents with amplitudes greater than 150 pA were used for further analysis. Global resolution estimations of cryo-EM density maps are based on the 0.143 Fourier Shell Correlation criterion[39]. The local resolution was estimated using cryoSPARC. The number of independent experiments (N) and the relevant statistical parameters for each experiment (such as mean or standard deviation) are described in the figure legends. No statistical methods were used to pre-determine sample sizes.

Reporting summary

Further information on research design is available in the Nature Portfolio Reporting Summary linked to this article.

Data availability

All of the cryo-EM maps and atomic coordinates produced from this study have been deposited into Electron Microscopy Data Bank and Protein Data Bank with accession numbers: hTRPC3 in complex with Nb1-94 (EMD-63868 [https://www.ebi.ac.uk/pdbe/entry/emdb/EMD-63868], PDB: 9U5C), hTRPC3 in complex with Nb1-25 (EMD-62268 [https://www.ebi.ac.uk/pdbe/entry/emdb/EMD-62268], PDB: 9KDB), hTRPC3 in complex with Nb3-37 (EMD-62269 [https://www.ebi.ac.uk/pdbe/entry/emdb/EMD-62269], PDB: 9KDC), GSK1702934A-bound hTRPC3 (EMD-62270 [https://www.ebi.ac.uk/pdbe/entry/emdb/EMD-62270], PDB: 9KDD), and 4n-bound hTRPC3 (EMD-62271 [https://www.ebi.ac.uk/pdbe/entry/emdb/EMD-62271], PDB: 9KDE). The entries 7DXB, 6CUB, 7DXF, 7DXG, 7D4P, and 6UZ8 used in this study were

downloaded from the Protein Data Bank. The lipidomics data generated in this study have been deposited in the MetaboLights under the Study ID MTBLS12881. Source data are provided with this paper. All data supporting the results of this study can be found in the article, supplementary, and source data files. Source data are provided with this paper.

References

1. Wang, H. et al. TRPC channels: structure, function, regulation and recent advances in small molecular probes. *Pharmacol. Ther.* **209**, 107497 (2020).
2. Hofmann, T. et al. Direct activation of human TRPC6 and TRPC3 channels by diacylglycerol. *Nature* **397**, 259–263 (1999).
3. Beck, B. et al. TRPC7 is a receptor-operated DAG-activated channel in human keratinocytes. *J. Invest. Dermatol.* **126**, 1982–1993 (2006).
4. Storch, U. et al. Dynamic NHERF interaction with TRPC4/5 proteins is required for channel gating by diacylglycerol. *Proc. Natl. Acad. Sci. USA* **114**, E37–E46 (2017).
5. Zhu, X. et al. trp, a novel mammalian gene family essential for agonist-activated capacitative Ca2+ entry. *Cell* **85**, 661–671 (1996).
6. Riccio, A. et al. mRNA distribution analysis of human TRPC family in CNS and peripheral tissues. *Brain Res. Mol. Brain Res.* **109**, 95–104 (2002).
7. Reiser, J. et al. TRPC6 is a glomerular slit diaphragm-associated channel required for normal renal function. *Nat. Genet.* **37**, 739–744 (2005).
8. Winn, M. P. et al. A mutation in the TRPC6 cation channel causes familial focal segmental glomerulosclerosis. *Science* **308**, 1801–1804 (2005).
9. Fan, C., Choi, W., Sun, W., Du, J. & Lu, W. Structure of the human lipid-gated cation channel TRPC3. *Elife* **7** https://doi.org/10.7554/eLife.36852 (2018).
10. Tang, Q. et al. Structure of the receptor-activated human TRPC6 and TRPC3 ion channels. *Cell Res.* **28**, 746–755 (2018).
11. Guo, W. et al. Structural mechanism of human TRPC3 and TRPC6 channel regulation by their intracellular calcium-binding sites. *Neuron* **110**, 1023–1035 e1025 (2022).
12. Bai, Y. et al. Structural basis for pharmacological modulation of the TRPC6 channel. *Elife* **9**, e53311 (2020).
13. Nakamura, Y. & Fukami, K. Regulation and physiological functions of mammalian phospholipase C. *J. Biochem.* **161**, 315–321 (2017).
14. Lichtenegger, M. et al. An optically controlled probe identifies lipid-gating fenestrations within the TRPC3 channel. *Nat. Chem. Biol.* **14**, 396–404 (2018).
15. Erkan-Candag, H. et al. Diacylglycerols interact with the L2 lipidation site in TRPC3 to induce a sensitized channel state. *EMBO Rep.* **23**, e54276 (2022).
16. Song, K. et al. Structural basis for human TRPC5 channel inhibition by two distinct inhibitors. *Elife* **10** https://doi.org/10.7554/eLife.63429 (2021).
17. Xu, X. et al. Characterization of small molecule TRPC3 and TRPC6 agonist and antagonists. *Biophys. J.* **104**, 454a (2013).
18. Qu, C. et al. Pyrazolopyrimidines as potent stimulators for transient receptor potential canonical 3/6/7 channels. *J. Med. Chem.* **60**, 4680–4692 (2017).
19. Yang, P. L. et al. GSK1702934A and M085 directly activate TRPC6 via a mechanism of stimulating the extracellular cavity formed by the pore helix and transmembrane helix S6. *J. Biol. Chem.* **297**, 101125 (2021).
20. Svobodova, B. et al. A single point mutation in the TRPC3 lipid-recognition window generates supersensitivity to benzimidazole channel activators. *Cell Calcium* **79**, 27–34 (2019).
21. Wills, R. C. & Hammond, G. R. V. PI(4,5)P2: signaling the plasma membrane. *Biochem. J.* **479**, 2311–2325 (2022).
22. Ueda, Y., Ishitsuka, R., Hullin-Matsuda, F. & Kobayashi, T. Regulation of the transbilayer movement of diacylglycerol in the plasma membrane. *Biochimie* **107**, 43–50 (2014).
23. Gonzales, D. T. et al. Quantifying single-cell diacylglycerol signaling kinetics after uncaging. *Biophys. J.* **123**, 921–927 (2024).
24. Poursharifi, P., Madiraju, S. R. M. & Prentki, M. Monoacylglycerol signalling and ABHD6 in health and disease. *Diabetes Obes. Metab.* **19**, 76–89 (2017).
25. Zhao, S. et al. alpha/beta-Hydrolase domain-6-accessible monoacylglycerol controls glucose-stimulated insulin secretion. *Cell Metab.* **19**, 993–1007 (2014).
26. Hansen, H. S., Rosenkilde, M. M., Holst, J. J. & Schwartz, T. W. GPR119 as a fat sensor. *Trends Pharmacol. Sci.* **33**, 374–381 (2012).
27. Rached, G. et al. TRPC3 regulates islet beta-cell insulin secretion. *Adv. Sci. (Weinh.)* **10**, e2204846 (2023).
28. Guo, W., Wang, M. & Chen, L. A co-expression vector for baculovirus-mediated protein expression in mammalian cells. *Biochem. Biophys. Res. Commun.* **594**, 69–73 (2022).
29. Phulera, S. et al. Cryo-EM structure of the benzodiazepine-sensitive α1β1γ2S tri-heteromeric GABA(A) receptor in complex with GABA. *Elife* **7** https://doi.org/10.7554/eLife.39383 (2018).
30. Zhang, J. et al. Clean transfer of large graphene single crystals for high-intactness suspended membranes and liquid cells. *Adv. Mater.* **29** https://doi.org/10.1002/adma.201700639 (2017).
31. Patel, A., Toso, D., Litvak, A. & Nogales, E. Efficient graphene oxide coating improves cryo-EM sample preparation and data collection from tilted grids. Preprint at https://www.biorxiv.org/content/10.1101/2021.03.08.434344v1 (2021).
32. Zheng, S. Q. et al. MotionCor2: anisotropic correction of beam-induced motion for improved cryo-electron microscopy. *Nat. Methods* **14**, 331–332 (2017).
33. Zhang, K. Gctf: real-time CTF determination and correction. *J. Struct. Biol.* **193**, 1–12 (2016).
34. Zivanov, J. et al. New tools for automated high-resolution cryo-EM structure determination in RELION-3. *Elife* **7** https://doi.org/10.7554/eLife.42166 (2018).
35. Punjani, A., Rubinstein, J. L., Fleet, D. J. & Brubaker, M. A. cryoSPARC: algorithms for rapid unsupervised cryo-EM structure determination. *Nat. Methods* **14**, 290–296 (2017).
36. Wang, N. et al. Structural basis of human monocarboxylate transporter 1 inhibition by anti-cancer drug candidates. *Cell* **184**, 370–383 e313 (2021).
37. Emsley, P., Lohkamp, B., Scott, W. G. & Cowtan, K. Features and development of Coot. *Acta Crystallogr. D. Biol. Crystallogr.* **66**, 486–501 (2010).
38. Adams, P. D. et al. PHENIX: a comprehensive Python-based system for macromolecular structure solution. *Acta Crystallogr. D. Biol. Crystallogr.* **66**, 213–221 (2010).
39. Chen, S. et al. High-resolution noise substitution to measure overfitting and validate resolution in 3D structure determination by single particle electron cryomicroscopy. *Ultramicroscopy* **135**, 24–35 (2013).

Acknowledgements

We thank all of the Chen Lab members for their kind help. We thank Dr. Xiaolin Zhang at Dizal Pharmaceutical Company for providing BTDM and 4n compounds. Cryo-EM data collection was supported by the Electron Microscopy Laboratory and the Cryo-EM platform of Peking University. Part of the structural computation was also performed on the Computing Platform of the Center for Life Science and High-performance Computing Platform of Peking University. We thank the National Center for Protein Sciences at Peking University in Beijing, China, for assistance with negative stain EM. The work is supported by grants from the Ministry of Science and Technology of China (National Key R&D Program of

China, 2022YFA0806504 to L.C.), National Natural Science Foundation of China (32225027 to L.C., 52021006 to H.P., 32301009 to W.G.), and the Center for Life Sciences (CLS to L.C.). W.G. is supported by the postdoctoral foundation of the Peking-Tsinghua Center for Life Sciences, Peking University (CLS).

Author contributions

L.C. initiated the project. Y.C. carried out electrophysiological experiments. J.Z., W.G. and Y.C. purified the protein, prepared the cryo-EM sample, processed the data and built the model. J.Z., W.G., J.X. and M.W. collected the cryo-EM data. Y.C. and L.Q. conducted the mass spectrum experiments. M.Z. and Y.W. generated nanobodies. H.P. and X.Z. prepared the graphene-coated grids. All authors contributed to the manuscript preparation.

Competing interests

Min Zhu and Yakun Wan are employees of Shanghai Novamab Biopharmaceuticals Co., Ltd. The remaining authors declare no competing interests.

Additional information

Supplementary information The online version contains supplementary material available at https://doi.org/10.1038/s41467-025-64435-6.

Correspondence and requests for materials should be addressed to Lei Chen.

Peer review information *Nature Communications* thanks the anonymous reviewers for their contribution to the peer review of this work. A peer review file is available.